An Improved Level Set for Liver Segmentation and Perfusion Analysis in MRIs

Gang Chen, Lixu Gu, *Member, IEEE*, Lijun Qian, and Jianrong Xu

***Abstract*—Determining liver segmentation accurately from MRIs is the primary and crucial step for any automated liver perfusion analysis, which provides important information about the blood supply to the liver. Although implicit contour extraction methods, such as level set methods (LSMs) and active contours, are often used to segment livers, the results are not always satisfactory due to the presence of artifacts and low-gradient response on the liver boundary. In this paper, we propose a multiple-initialization, multiple-step LSM to overcome the leakage and over-segmentation problems. The multiple-initialization curves are first evolved separately using the fast marching methods and LSMs, which are then combined with a convex hull algorithm to obtain a rough liver contour. Finally, the contour is evolved again using global level set smoothing to determine a precise liver boundary. Experimental results on 12 abdominal MRI series showed that the proposed approach obtained better liver segmentation results, so that a refined liver perfusion curve without respiration affection can be obtained by using a modified chamfer matching algorithm and the perfusion curve is evaluated by radiologists.**

***Index Terms*—Level set methods (LSMs), liver perfusion analysis, liver segmentation, multiple initializations.**

I. Introduction

LIVER PERFUSION is a quantitative measurement of the blood flow in the liver, and plays an important role in providing information for the assessment and treatment of various liver diseases. For example, it can be used as a noninvasive and repeatable technique in assessing the probability of acute rejection in liver transplants [1]. By injecting a contrast agent into blood vessels of the liver while taking abdominal MRIs in fixed time intervals, the concentration of the contrast agent can be recorded as a perfusion curve. However, in a clinical setting, the main challenge is the liver motion due to the patient's respiration during the liver perfusion procedure, which causes fluctuation of the perfusion curve's position across the image series and adversely affects the appearance of the perfusion curve. Since it is impractical to ask patients to hold their breaths during the lengthy procedure, the attending radiologist must manually mark the perfusion position across the entire image series, which is tedious and time-consuming. Therefore, there is an urgent need to automate the liver perfusion analysis and measurement process. However, we must first achieve precise liver segmentation before attempting any automatic liver perfusion analysis [2], [3].

Medical image segmentation is an important research topic that is widely used in 2-D and 3-D visualizations of patients' internal structures, enhancing diagnostics and allowing detailed preplanning of surgeries. Among the various medical image segmentation methods, level set methods (LSMs), which are based on the representation and evolution of curves or surfaces, play an important role. They can handle cavities, concavities, splitting/merging, and convolution [4]. A good discussion of medical image segmentation algorithms, including LSM, can be found in [5]. Malladi and Sethian [6] introduced the usage of curvature, and the gradient of the image convolved with a Gaussian as a potential field to guide the evolution of the level set function. Our segmentation research is inspired by their work; multiple initializations and a redefined speed function are introduced into the level set propagation to handle the weak boundaries in MR liver images.

So far, much research [7]–[16] has focused on liver segmentation in Computed tomography (CT) images, but only a few of them address MRI. The main reason is that abdominal MRIs have more artifacts affected and a low gradient response, which makes precise liver segmentation very challenging. The watershed transform was first applied to the image gradient magnitude in [7], and the result is used as the initial curve in the following level set segmentation methods, resulting in smooth and accurate liver contours from CT images. Similarly, the authors in [8] employed a topology-adaptive snake algorithm to segment liver tissues from CT image slices, avoiding the leakage problem by adding an inflationary force to the basic snake equation and initializing the snake inside the liver. Another study using the snake method is listed in [9], where an improved gradient vector flow (GVF) snake [10], [11] was proposed in order to produce an edge map by a Canny edge detector, with final modifications using a liver template and a concavity removal algorithm combined in segmentation. The authors of [12] proposed a liver segmentation method that utilizes texture-based low-level features, with the segmentation results compared against three different texture extraction methods: co-occurrence matrices, Gabor filters, and Markov random fields [13]. Lim *et al.* [14] proposed an approach based on the intensity distribution of multiple abdominal CT samples, and then utilized a recursive morphological filter with region-labeling and clustering to detect the liver's search range and generate the initial liver contour. Recently,

Manuscript received August 13, 2007; revised May 25, 2008. First published October 31, 2008; current version published January 4, 2009. This work was supported in part by the Chinese National Natural Science Foundation under Grant 30770608 and in part by the National Fundamental Research Program (973) under Grant 2006CB504801 and Grant 2007CB512701.

G. Chen and L. Gu are with the Image Guided Surgery and Therapy Laboratory, Med-X Research Institute and Department of Computer Science, Shanghai Jiao Tong University, Shanghai 200030, China (e-mail: gu-lx@cs.sjtu.edu.cn).

L. Qian and J. Xu are with the Radiology Department, Renji Hospital, Shanghai Jiao Tong University, Shanghai 200030, China (e-mail: xujianr@online.sh.cn).

Color versions of one or more of the figures in this paper are available online at http://ieeexplore.ieee.org.

Digital Object Identifier 10.1109/TITB.2008.2007110

statistics- and atlas-based segmentation methods were also introduced. The authors of [15] proposed a two-step automatic liver segmentation method. First they evolved a rough extracted liver boundary based on MAP estimation from a probability atlas of the liver, and then, precisely segmented the liver using an LSM. Another atlas-based liver segmentation method for 3-D CT images is introduced in [16], where a voxel-based segmentation with probabilistic atlas is employed to obtain an initial liver region for precise segmentation using a statistical shape model. Heimann *et al.* [17] employed an active shape model (ASM) to segment the liver region in CT scans, where a statistics shape model was built from 32 samples using an optimization approach based on the minimum description length representation. Regarding MRI segmentation, Sebastian and Gu [2] model the liver perfusion problem using a registration method, where a fast marching method (FMM) and an LSM [4]–[6] were used to segment the liver region roughly from MRI slices, after which a distance vector transform was employed to identify the perfusion position along the time sequence images. However, we must note that the method can segment only a part of the liver region and may lead to leakage and over-segmentation. An active contour model [18], [19] was proposed in [3] to segment the liver region and chamfer matching (CM) [20], [21] was applied to align the slices in an MRI series, with a prior liver shape image required to help extract the liver shape and remove artifacts and redundancy. Unfortunately, this prior shape must be manually segmented in advance for every MRI series. Another improved LSM that aimed to solve the leakage problem is presented in [22]. The authors defined the speed function from a local homogeneity measurement instead of a gradient base, but the process is slow and does not yield promising results in some MRIs. This method is used in our experimental comparison for performance evaluations. From this brief literature review, it is obvious that although some research addresses liver segmentation in both CT and MR images, and some attempts at automatic liver perfusion analysis were reported, only a few provide promising outcomes automatically or at relatively low cost.

In this paper, a four-step liver segmentation scheme is introduced to efficiently track precise perfusion positions along the time series of MRIs. The concept of multiple initializations is combined with a convex hull (CH) algorithm to improve the traditional LSM and prevent leakage and over-segmentation, which can be easily extended to further initializations upon the shape and topology of the region of interest (ROI), and can be computed in parallel. Furthermore, a modified CM method is introduced to better serve liver perfusion analysis by helping radiologists automatically track the liver's perfusion position under respiration.

The remainder of this paper is organized as follows. In Section II, after a quick review of the traditional LSM and FMM, the CH and CM algorithms are introduced. The details of the four-step multiple-initialization LSMs are presented in Section III, and Section IV covers the automated liver perfusion analysis. In Section V, the methods are validated and discussed by presenting the results of multiple experiments, with conclusions presented in Section VI.

II. Algorithm Review

A. Level Set and Fast Marching Methods

In this section, we briefly review the LSM, its narrow-band implementation, and the FMM. The LSM is a numerical technique that follows the evolution of interfaces. It represents the interface as a level set of a higher dimensional function, such as the signed distance to the interface, where the zero crossings of the function values represent the original interface. The evolution of the interface in the initial value problem can be represented by the equation $\phi_t + F|\nabla\phi| = 0$, where ϕ is the embedding function, ϕ_t is its time derivative, and F is the speed function. There are many advantages to this formulation: one is that ϕ remains a function as long as F is smooth, so it can handle broken, merged, and changed topologies. Another advantage is that geometric properties of the curve are easily determined from a particular level set of the surface. One can observe that the evolving curve is moved by updating the level set function at a small set of points in the neighborhood of the zero level set. By updating ϕ only in a narrow band around the curve, one can reduce the computational complexity from $O(N^3)$ to $O(N^2)$. This procedure is known as a narrow-band LSM [23].

As a predigest version of LSM, the FMM [4] can efficiently solve curve and surface evolution problems. It calculates the arrival time of a given point (x, y) on a closed curve that evolves under a fixed-sign normal speed $F(x, y)$. Because of the fixed-sign speed, the evolving curve's movement can only expand or shrink, which makes FMM faster than LSM. The Eikonal equation can be written as $|\nabla T|F = 1$, where $T(x, y)$ is the arrival time of point (x, y). The FMM explicitly constructs the solution for all points in the computation domain, and is of complexity $O(N\log(N))$.

B. Convex Hull Algorithm

The CH problem [24] is one of the most fundamental problems in computational geometry: given a set S of n points in the plane, find the convex hull of S:CH(S). We solved this problem using the well-known geometric sweeping algorithm called "Graham scan" [25], with the complexity $O(N\log(N))$. This algorithm is employed in our multistep LSM to combine partial liver regions efficiently, with more details given in Section III.

C. Chamfer Matching Match

The CM, first introduced by Barrow *et al.* [20], is a method that matches edge points or other low-level feature points extracted from a 2-D image. There are two binary images involved in the process. One is a source image in the form of a distance map; another is a template image containing the object's shape contour. The template image performs a rigid transformation to make its shape contour overlap with the boundary region in the source image. An average value of the overlapped pixels in the source image is the measure of the correspondence between them, where a perfect match means that the average value is close to zero. Transformations with different parameters are applied and the one with the minimum average is selected. Often

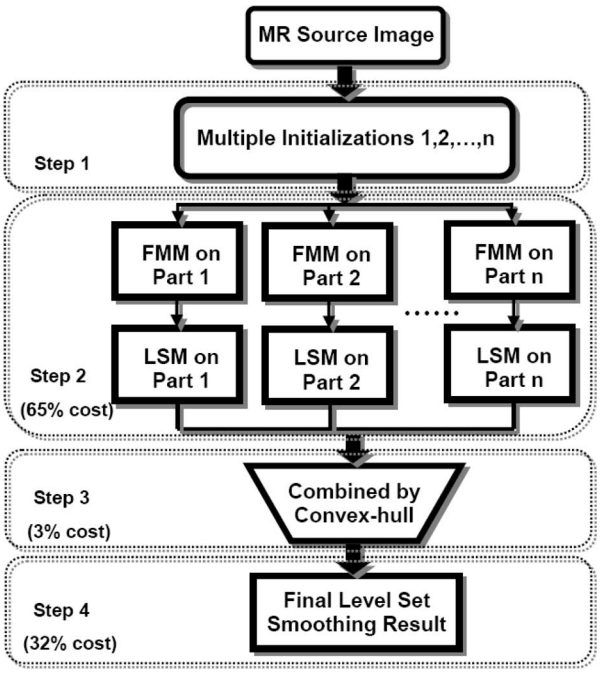

Fig. 1. Flowchart of the proposed four-step multiple-initialization LSM approach, where the cost distribution is inspected and specified.

the rms average distance is used as the measure

$$\text{rms} = \frac{((v_1^2 + v_2^2 + \ldots + v_N^2)/N)^{1/2}}{3}. \quad (1)$$

Here, v_i is the ith pixel of the source image that is within the segmented liver region and N is the number of pixels.

III. Multiple-Step Level Set Segmentation Method

As shown in Fig. 1, the improved LSM consists of four steps. First, multiple cycles are user-defined as the initial curves for the FMM and LSM, although all the images in one series can share the same set of initial cycles. Second, parallel propagations using FMM and LSM based on these initial curves are implemented. The third step involves a combination of the partial segmentation results using a CH algorithm. The combined rough liver contour is then used as the initial curve for the next step. The fourth step is to smooth the primary liver contour using LSM, where a new speed function is employed to create a nearly CH for the zero level set. The total computation time is measured in seconds, and exhibits higher cost in step 2 (65%) and step 4 (32%).

A. Multiple Initializations

In the improved LSM, multiple seeds that mark the initial curves must be placed at different points of the ROI manually. Specifically, if we consider the region roughly of a polygonal shape, it is reasonable to set the initial seeds near the center of each corner. The initial curves then evolve under the force of FMM and LSM to partially trace the rough shape of the liver. Level set zero crossings represent the original interface with a signed distance function ϕ for a fixed point $u_0(x, y)$, which is defined as

$$\phi(x,y) = \begin{cases} |(x_{u_0}, y_{u_0}) - (x_p, y_p)|, & \text{if } u_0(x,y) \text{ is not in the interface} \\ -|(x_{u_0}, y_{u_0}) - (x_p, y_p)|, & \text{otherwise.} \end{cases} \quad (2)$$

Here, $P(x, y)$ is one of the nearest points from $u_0(x, y)$ on the interface. We can obtain a series of signed distance functions $\phi_0^1, \phi_0^2, \ldots, \phi_0^n$ (where n is the number of cycles) that represent the multiple initializations. Among the same MRI series, the sequence can share the initializations. This claim is based on the following observations: the movement of the liver is mostly in vertical and the rotation can be ignored. The inner organ's rotation and deformation due to respiration is a very delicate problem [26], and it needs a time-consuming rigid and nonrigid registration algorithm to compensate for the respiration effect [27]. After investigating the rotation problem, we decided to ignore it. Our experiment result showed that the rotation effect was always very limited. From prior experimentation, two or three initialization cycles are enough to effectively cover the whole liver in abdominal MRIs. If only one cycle is used, part of the evolving curve may lead to leakage long before others reach the desired boundary, which is the main drawback of traditional LSMs. We shall demonstrate this in Section V.

B. Parallel Segmentation Using FMM and LSM

Once we have the initial curves, FFM and LSM are used to evolve the curve. Here, we focus on the improvement of the speed function, which defines the interface propagation speed in the normal direction and the stopping criteria. The base speed function depends on the gradient of image u_0 [28], [29]. It is defined as

$$F_{\text{base}}(u_0) = \frac{1}{1 + |\nabla G_\sigma(x,y) * u_0(x,y)|^p}, \qquad p \geq 1 \quad (3)$$

where $\nabla G_\sigma(x, y) * u_0(x, y)$ is the convolution of u_0 with Gaussian filter

$$G_\sigma = \sigma^{-1/2} e^{-(x^2+y^2)/4\sigma}. \quad (4)$$

FMM is employed initially to quickly evolve the multiple curves in parallel. The mean FMM iteration number is experimentally set to 20 to prevent the over-segmentation, if any. After F_{base} becomes zero or the curve stops evolution at the last iteration, we get a group of new distance functions: $\phi^1, \phi^2, \ldots, \phi^n$. To fine-tune the curves, we switch to level set propagation, where every ϕ^i is defined as

$$\phi_t^i + F|\nabla\phi| = 0. \quad (5)$$

Here, ϕ_t^i is the ith evolving curve's derivative over time t and F is the new speed function, which is defined as

$$F(x,y,t) = \alpha - \kappa_{x,y,t} + F_{\text{base}}(x,y). \quad (6)$$

It includes a local curvature term $\kappa_{x,y,t}$ and a force term $F_{\text{base}}(x, y)$, where the curvature controls the smoothness of the evolving curve when the force term guides the curve to the desired boundary. By updating each ϕ^i in a narrow band around the curve, we can reduce the computational complexity from

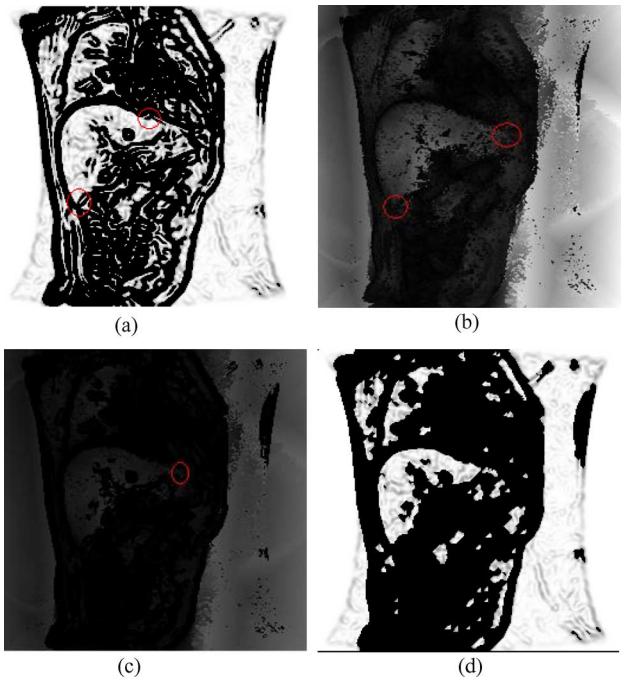

Fig. 2. Different speed images. (a) Traditional LSM's speed image. (b) Jin *et al.*'s [22] speed image. (c) Traditional LSM's speed image added to Jin *et al.*'s [22]. (d) Our opened speed image. The cycles are possible areas that will lead to leakage.

$O(N^3)$ to $O(N^2)$, where the narrow-band size is experimentally set to 6 to achieve a better result. In order to speed up the algorithm even more, we can employ multithread programming or a multicore CPU to make full use of the algorithm's parallelization ability.

We have mentioned that FMM and LSM are prone to leakage and over-segmentation problems. This is mostly because of the definition of the traditional speed function. The authors in [22] proposed using local homogeneity measurements to produce the speed function, but this is very time-consuming. Our solution is to apply an *open* operation to the traditional speed image. The *open* operation on image A using a 3×3 cross shape structuring element B is denoted by

$$A \circ B : A \circ B = (A \ominus B) \oplus B \tag{7}$$

where $\oplus$ and $\ominus$ denote morphological dilation and erosion operations, respectively. After the *open* operation, most of the noise in the speed image is removed, so the level set's evolving curve will stop at the proper position instead of evolving the noise. This not only limits the risk of leakage in each parallel segmentation step, but also produces a high probability that the segmentation may not cover the entire shape. The CH algorithm can help to solve this problem in the following step. Fig. 2 shows an example of the four different speed images, where in Fig. 2(c), the speed function of the traditional LSM is added to Jin *et al.*'s [22] speed function. It adds the low-intensity part of the traditional level set speed image to Jin *et al.*'s [22] in order to reduce the noises.

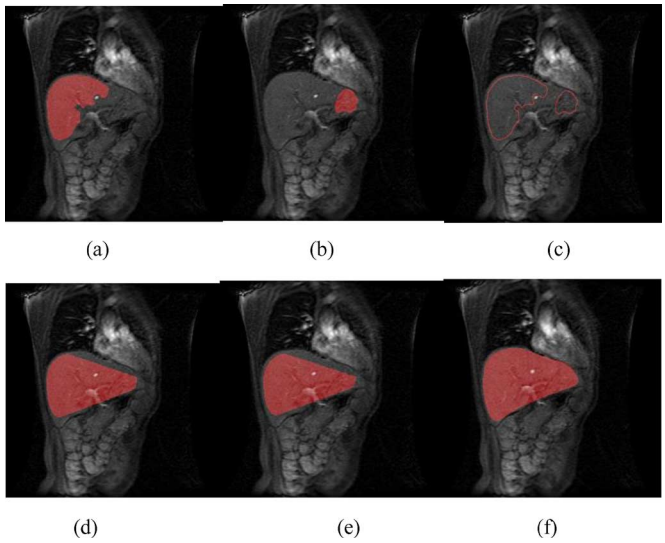

Fig. 3. Example of the liver segmentation using two initial curves. (a) Left segmented result. (b) Right segmented result. (c) Before CH. (d) Highlighted CH liver region before erosion operation. (e) Highlighted CH liver region after erosion operation. (f) Level set smoothed result.

C. Combine Partial Segmentation using CH

So far, we have obtained n segmented partial liver regions, which must be combined into the seed of the next level set smoothing step. The CH [24], [25] algorithm is employed to solve this combination by using the geometric sweeping algorithm known as the "Graham scan." First, the edge points of each partial curve are used as the input to the CH algorithm, which consists of first detecting extreme points as pivots, then sorting the points in order of increasing angle about the pivot, and finally hull building. Thereafter, the combined contour is shrunken twice by morphological erosion using a 3×3 cross shape structuring element to keep it stable and leak-free in the next level set smoothing step. Finally, the partial segmentation results are incorporated into the result to compensate for lost pixels during the shrinkage process. The obtained partial liver boundary from the previous steps remains nearly unchanged after the CH algorithm, while the new parts of boundary induced by CH will be refined by the next step to fit the real boundary. An example of the procedure is shown in Fig. 3.

D. Level Set Smoothing Step

The final step is to refine the liver segmentation by smoothing the primary CH result to get a better liver contour. Here the speed image is the original one without *open* operation, and the definition of $F(x, y, t)$ is simplified, with only the curvature term to prevent leakage:

$$F_{\text{hull}}(x, y, t) = \begin{cases} -1.5\kappa_{x,y,t}, & \text{if } \kappa_{x,y,t} < 0 \\ -0.1\kappa_{x,y,t}, & \text{if } \kappa_{x,y,t} \geq 0. \end{cases} \tag{8}$$

The speed function $F_{\text{hull}}(x, y, t)$, which forces curves to move along the normal direction, is calculated by the local curvature $\kappa_{x,y,t}$. If $\kappa_{x,y,t}$ is negative, the local shape is concave; otherwise, the local shape is convex. The parameters of

the speed function $F_{\text{hull}}(x, y, t)$ are defined by experiment, and the improved speed function can create a nearly CH of the zero level set in order to make the segmentation result smooth and leak-free. By making sure that the total number of pixels in the segmented region does not exceed a certain threshold, we can determine the stopping criteria of the level sets. This step is far less costly than step 2 because the contour is closer to the true liver boundary.

IV. Automatic Liver Perfusion Analysis

A modified CM algorithm is applied to the segmented liver regions to realize automatic liver perfusion analysis. In CM, the two input images are asymmetric. The source image is a distance map formed by assigning to each pixel the distance to the nearest edge pixel when the template image is a binary image containing the shape of the ROI. In our application, the level set evolving result is naturally a distance map and the template image is predefined where the perfusion position is marked manually. In other words, any slice of the same MR series can be selected as a template image. For example, we can select the segmentation result from the first slice as the template image, with its perfusion position defined by a radiologist. Because of the low quality of the MRI series, it is always difficult to fit a moving curve exactly to the liver boundary, and two modifications are applied here to guarantee precise outcomes. First, the noise component of the distance map, which remains in the same position across the image series, can be eliminated from the template image to protect the rms average. Second, the maximized number of hit edge pixels is introduced. After rigid transformation, when the template image is aligned with the source image, if the corresponding pixel in the source image is close to zero, our analysis indicates that the pixel lies on the boundary of the liver. The more of these so-called hit edge pixels there are, the better the two images are matched. Thus, letting v_i be the ith hit edge pixel for $i = 1, 2, \ldots, N$, we can find the maximum of following formula with respect to different rigid transformations:

$$F(N, v_i) = \frac{N}{((v_1^2 + v_2^2 + \cdots + v_N^2)/N)^{1/2}/3}. \tag{9}$$

We apply the X- and Y-axes' relative transformations dx_i and dy_i of the ith image to the perfusion positions x_0 and y_0 in template image, and (x_i, y_i), which is the position in the ith image, can be calculated by

$$\begin{cases} x_i = x_0 + dx_i \\ y_i = y_0 + dy_i. \end{cases} \tag{10}$$

The liver perfusion curve, obtained through a so-called dual-input single-compartment model [30], enables generation of series hepatic hemodynamic indexes such as hepatic blood flow (HBF), hepatic blood volume (HBV), hepatic arterial perfusion (HAP), portal vein perfusion (PVP), hepatic perfusion index (HPI), and mean transit time (MTT). These indexes give an integrated evaluation of the current condition of the liver and can characterize suspicious pathological changes. After multiple-initialization LSM segmentation and the CM, all the liver perfusion positions across the whole abdominal MRI series can be precisely located from the improved liver region, and the perfusion curve is thus depicted by recording the intensity variations.

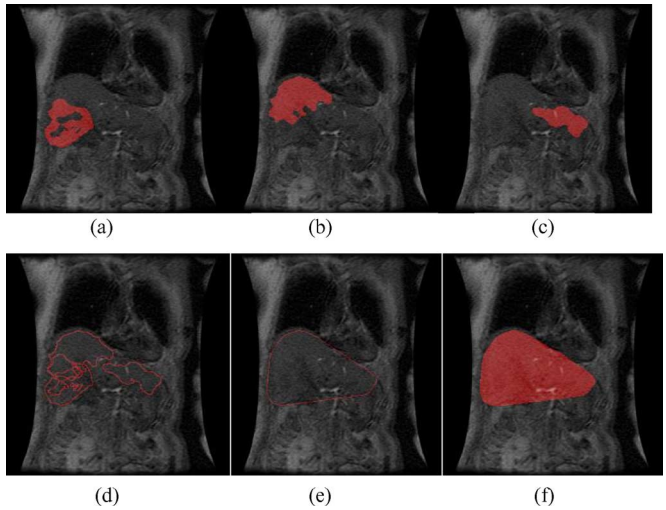

Fig. 4. Example of the liver segmentation using three initial curves. (a) First segmented result. (b) Second segmented result. (c) Third segmented result. (d) Total segmentation. (e) CH result. (f) Final segmentation result.

V. Experimental Results

We have implemented our improved multiple-initialization and multiple-step level set segmentation methods in C programming language and applied it to segment liver regions from abdominal MRIs, where the band size of the narrow-band LSM is 6. In order to evaluate our proposed algorithm, 12 perfusion series of 2-D abdominal MRIs with size of 256×256 are employed, and each dataset contains nearly 60 time sequenced slices. The datasets were scanned by a GE Medical Systems Genesis Sigma system at Shanghai Renji Hospital. They show the patients' abdomen in coronal view with relevant parameters: slice thickness 15.0; repetition time 4.7; echo time 1.2; magnetic field strength 15 000; and flip angle 60°. The experiments were performed on a PC with a Pentium-D 2700 MHz, 1-GB RAM. We also tested that our algorithm worked well with axial and sagittal images, which are of the same importance in clinics. The reason to present in coronal view is just because of the liver contours; however, in coronal images, it is considered more challenging as it is more likely to be misled by peripheral organs or other tissues, such as the heart, colon, small intestine, or diaphragm.

A. Segmentation of Liver From MRIs

Figs. 3 and 4 show the process examples of the improved LSM in segmenting the liver from MRIs, which employ two and three initial curves, respectively, in different MRI series. However, the numbers of initializations do not need to change in the same series. The number of initial circles is determined depending on the shape of the target region (the liver). Specifically, if we consider the region roughly as a polygonal shape, the number of edges is the maximal number of initial circles. It is suggested to locate the initial circles near the center of each angular corner.

Different segmenting stages using three initial circular curves are shown in Fig. 4, where the traditional LSM can hardly succeed due to the heavy artifacts and the unclear liver boundary. Here, our final segmented liver contour in Fig. 4(f) achieved reasonable details, and contains the vena cava and portal vein in the bottom of the liver. We keep the vessel regions for two reasons. First, the liver shape with these vessel regions appears smoother, which improves the accuracy of the CM to obtain a more precise perfusion position. Also, as 30% of a normal human liver's blood supply comes from the hepatic artery and 70% from the portal vein, the intensity of these vessels is essential for determining dynamic changes in the liver intensity, and they are significant in calculating perfusion indexes in our future research. Furthermore, the existence of these vessels is accepted by clinicians and will not influence the diagnosis.

Another example shown in Fig. 5 is used to compare our improved LSM to others in the literature, where traditional LSM, Chen and Gu's [3] active contours, and Jin *et al.*'s [22] LSM are used. We performed an extensive comparative study to show that the four-step approach of our multiple initializations is necessary. The first row in Fig. 5 shows that if the initialization curve of the traditional LSM is located at the left of the liver, it can only segment part of the liver. Adding more iteration steps would simply lead to leakage and over-segmentation. The same problems occur if the initialization curve is located at the right or in the middle of the liver, which are shown in the second row and the third row of Fig. 5. However, if we combine the first three rows of segmentation results before they get over-segmented, we can obtain a perfect segmentation. The fourth row in Fig. 5 shows that Jin *et al.*'s [22] algorithm cannot cover the whole liver and it is more costly (Table I). Although the result in the fifth row looks accurate, a prior liver shape must be first defined manually. The sixth row presents the proposed approach, in which most of the liver is segmented, except for slight under-segmentation in the lower left and lower right corners. This limitation arises because there is always a stronger gradient response in the upper half of the abdominal MRI series than in the lower half, so the evolving curve stops when it reaches the upper half liver boundary despite the fact that the lower half of the liver boundary has not been reached.

We also measured accuracy among these segmentation methods. The area-based measures [31], [32] are used to compare the regions enclosed by the segmentation boundary to an expert-defined gold standard. Let V_S and V_T represent the regions enclosed by the segmented boundary and the "true" boundary, respectively, and the true positive region (TP) as the region enclosed by both boundaries of $V_{\mathrm{TP}} = V_S \cap V_T$. In addition, the false positive (FP) and false negative (FN) are defined as $V_{\mathrm{FP}} = V_S - V_T$ and $V_{\mathrm{FN}} = V_T - V_S$, respectively [33]. The false fraction (FF) is one minus the fraction of falsely segmented regions. Thus, accuracy metrics can be defined as follows:

$$\text{TPF (true positive fraction)} = \frac{V_{\mathrm{TP}}}{V_T} \tag{11}$$

$$\text{FPF (false positive fraction)} = 1 - \frac{V_{\mathrm{FN}}}{V_T} \tag{12}$$

$$\text{FF (false fraction)} = 1 - \frac{V_{\mathrm{FP}} + V_{\mathrm{FN}}}{V_T}. \tag{13}$$

It is obvious that larger values of TPF, FPF, and FF correspond to higher segmentation accuracy. Fig. 6 shows the difference between the gold standard and the results from other four methods. The computing time and the accuracy analysis are listed in Table I, with the values averaged through all 60 time series images of the first dataset shown in Fig. 3. It reveals that out of the four candidates, both Chen and Gu's [3] active contours and the proposed approach achieved better segmentation results. However, the active contours approach requires previously manually defining a shape, whereas the proposed method needs only two initial seeds for an MRI series. Furthermore, the proposed method has the same order of magnitude for computation time as the traditional LSM, which achieves the fastest segmentation among all the candidates. The mean computing time for each slice of all the 12 MRI series is 8.56 s with standard deviation of 2.80. The comparison reveals that the improved multiple initialized LSM can better automate the segmentation of MRI liver regions while keeping the computing time fast enough for interactive segmentation. The overall accuracy analysis of all the 12 MRI series is shown in Fig. 7, where the mean TPF is 0.932 with standard deviation of 0.053, the mean FPF is 0.941 with standard deviation of 0.042, and the mean FF is 0.940 with standard deviation of 0.029. The seventh dataset shows lower accuracy due to the worse image quality.

B. Liver Perfusion Analysis

The performance of the automated liver perfusion analysis is tested against traditional techniques. An example is shown in Fig. 8. Compared to the traditional method (thin zigzag lines, fixed perfusion location), the proposed algorithm can track the movement of perfusion position across the whole series, providing a more accurate perfusion curve (thick smooth curve), with a Gaussian filter applied to get a smoothed perfusion curve. This filtering is acceptable because radiologists usually pay more attention to the trend rather than the exact value of each point in the curve. For example, a malignant tumor will present an early rapid ascending style because of the increasing blood supply by hepatic arteries, which helps in effective differential diagnosis. The error elimination provided by the Gaussian filter is properly handled in order not to affect the final result too much, an approach validated by radiologists from Shanghai Renji Hospital. To further investigate the accuracy of the proposed approach, the automated perfusion analysis result is verified by an expert-rectified result.

C. Summary

The proposed multiple-initialization LSMs can better segment regions with convex shape. Liver segmentation experiments from low-contrast abdominal MRIs show that the improved method is more accurate than the traditional LSM, and is much faster than others mentioned in Fig. 6.

The improved LSM is better poised to deal with low-contrast images than the traditional LSM because of its multiple initializations. The liver region is divided into two or three parts that are propagated independently to avoid sinking into local maxima and leakages. In comparison, due to the artifacts and low

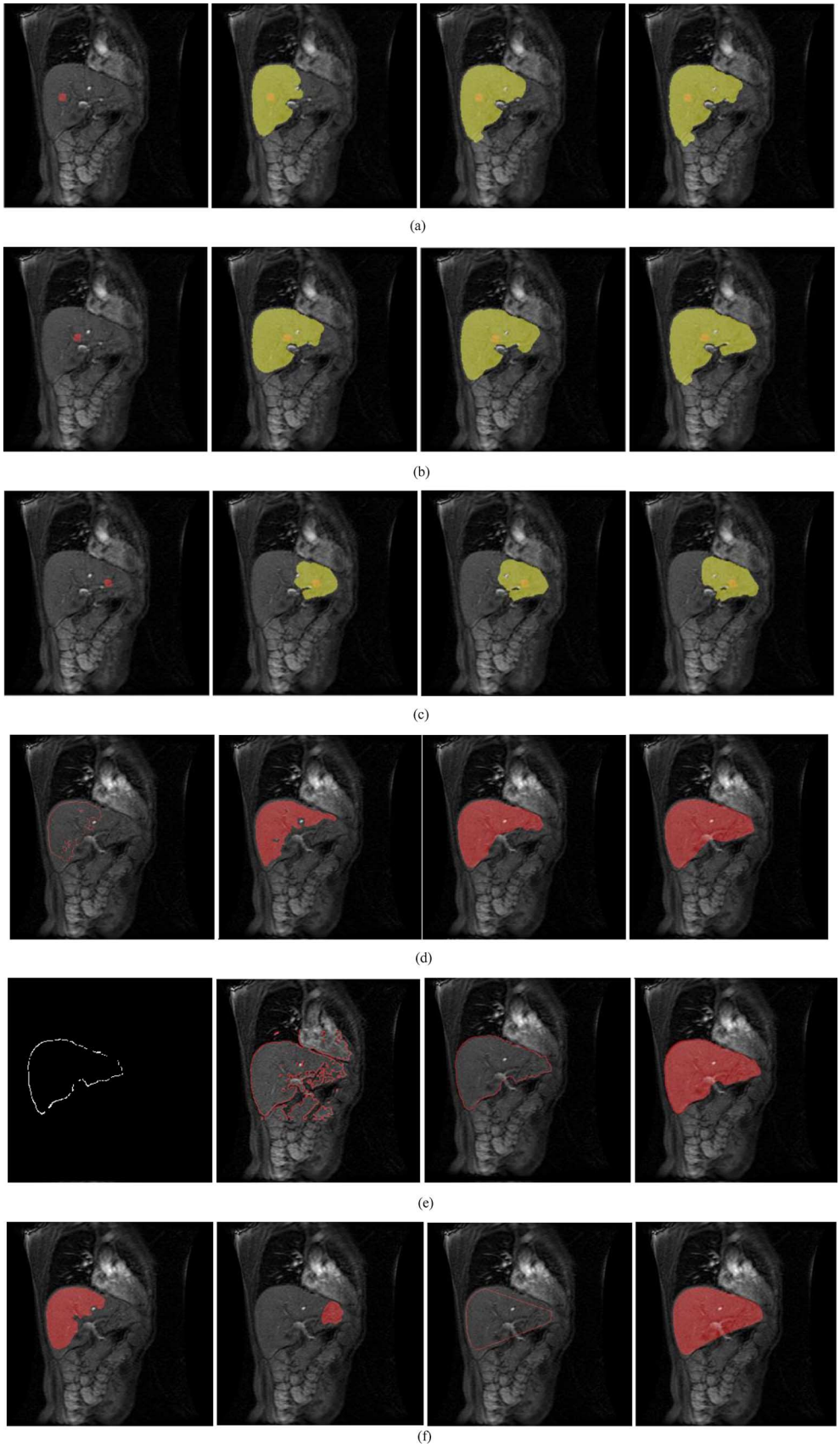

Fig. 5. Comparison among different liver segmentation methods from MRIs. (a) Traditional LSM, segmentation starting from the left. (b) Traditional LSM, segmentation starting from the middle. (c) Traditional LSM, segmentation starting from the right. (d) Jin *et al.*'s [22] LSM. (e) Chen and Gu's [3] active contours method; from left to right are edge pixels, the active contour's result, complete liver contours by connecting edge pixels, and the final result. (f) Our improved multiple LSM; from left to right are the left partial and right partial segmentation results, CH result, as well as the final segmentation result.

TABLE I
MEAN COMPUTING TIME AND ACCURACY ANALYSIS

Segmentation Method	Manual Work	Seeds Number	Average Time	TPF	FPF	FF
Tradition	less	1	4.92s	0.783	0.855	0.847
Jin's[22]	less	1	202.14s	0.886	0.928	0.923
Chen's[3]	more	1	16.34s	0.981	0.981	0.979
Our method	less	2 or 3	7.92s	0.950	0.961	0.958

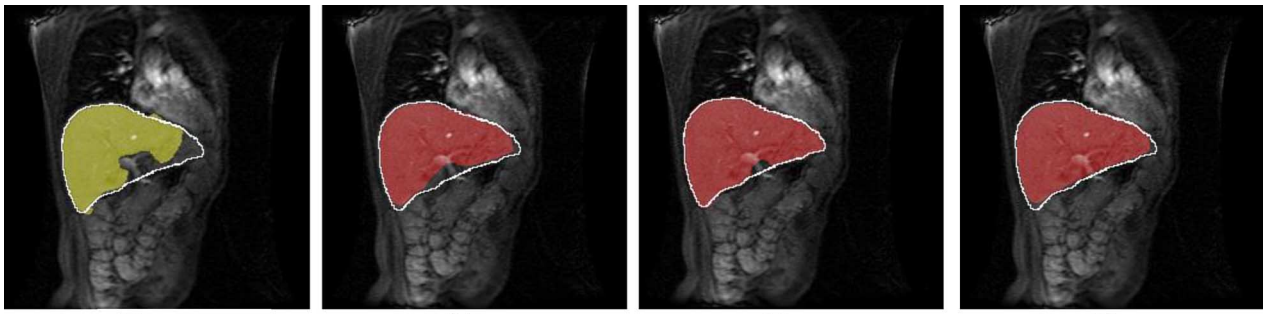

(a) (b) (c) (d)

Fig. 6. Difference between the gold standard and each of the four algorithm results. (a) Traditional LSM. (b) Jin *et al.*'s [22] LSM. (c) Chen and Gu's [3] active contours. (d) Our improved multiple-initialization LSM result. White lines indicate the expert-defined gold standard.

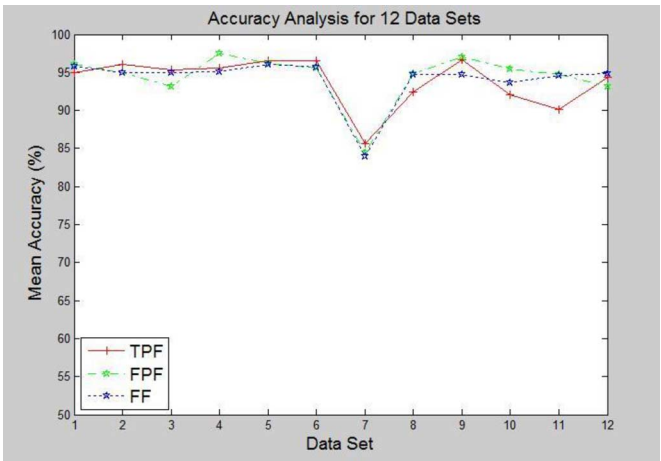

Fig. 7. Mean segmentation accuracy of the 12 datasets. The mean TPF is 0.932 with standard deviation of 0.053, the mean FPF is 0.941 with standard deviation of 0.042, and the mean FF is 0.940 with standard deviation of 0.029. The seventh dataset shows lower accuracy due to the worse image quality.

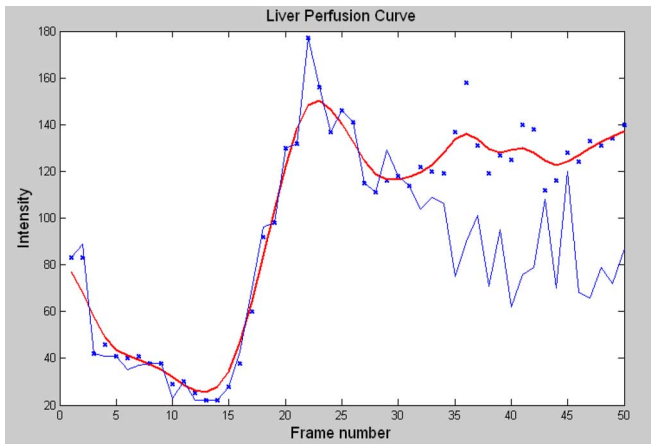

Fig. 8. Liver perfusion intensity curve. Points labeled by "x" are obtained by the proposed method, where they are normalized by Gaussian filter to the red curve. It is compared to the result of the original method using a fixed position across the whole series shown in blue lines.

gradient of the liver boundary in MRIs, the traditional LSM, which starts from only one seed, easily results in leakage problems before the other parts of evolving curve reach the boundary. The separate regions from the multiple initializations can be combined by using the CH algorithm, and another global level set smoothing is applied to the CH result to further evolve the curve to the true boundary without taking risk. The improved LSM can be easily extended to more initializations according to the shape and topology of the ROI and the image quality. Furthermore, this framework has great potential for parallel computing to accelerate the heavy processing especially involved in 3-D image analysis.

The main drawback of the multiple-initialization LSM method is the difficulty in automatically determining the number of initializations. Meanwhile, the under-segmentation problem still exists on lower sharp corner regions due to the low-gradient definition of the lower half of the liver region in the abdominal MRIs.

From the experimental results, we find that the complexity of multiple-initialization LSM is of the same order of magnitude as those of the traditional LSM. Although more steps are introduced into our multiple-step approach, as described in Section III, the improved LSMs do not introduce much more extra effort than the traditional LSM as well as benefit from parallel implementation in the second step. Both our improved LSM

and Jin *et al.*'s [22] improved LSM aim at solving the leakage problem, but our multiple-initialization LSM is much faster.

The multiple-initialization LSM can cover more liver regions before leakage and over-segmentation occur than does tradition LSM, especially when dealing with abdominal MRIs with heavy artifacts and weak boundaries. From Table I, we can find that it is more accurate than Jin *et al.*'s [22] LSM, and is comparable in accuracy to Chen and Gu's [3] active contours segmentation result.

The multiple-initialization LSM requires less user interaction, except during the definitions of the initialization cycles and the perfusion position. By comparison, the higher accuracy of liver segmentation in Chen and Gu's [3] method is dependent on more manual definitions to construct a complete liver template for each datasets.

VI. Conclusion

In this paper, a novel multiple-initialization LSM approach is proposed to overcome the leakage and over-segmentation problems in segmenting the liver region from MRIs. An automated liver perfusion analysis method is also proposed to automatically conclude liver perfusion curves and compensate for patient respiration. The segmentation method has been tested on 12 series of 2-D abdominal MRIs, where the results reveal that the proposed method has the potential to segment the liver region quickly and accurately even from images with more artifacts and lower gradient responses on the boundaries. The accuracy of the proposed method is significantly improved from one of the traditional LSMs. The relationship between leakage and level set's speed function was also examined. The comparisons against the traditional LSM, Chen and Gu's [3] active contour method, and Jin *et al.*'s [22] method show that the improved approach yields better performance even with limited user interaction.

Relying on the stability of the shape of the liver, modified CM can be used to automatically locate relative perfusion positions across abdominal MRIs, as verified in the experiment. A refined liver perfusion curve without respiration effects can thus be obtained.

In the future, we plan to estimate the optimal number of initializations by texture analysis, work even harder to further improve segmentation accuracy without user interaction, solve the slight under-segmentation for other potential applications like volumetry or morphometry, the segmentation approach to other organs, and extend it to 3-D volume data.

Acknowledgment

This work was inspired by N. Sebastian's important work on liver perfusion and his implementation of traditional LSMs. The authors are grateful to S. Nowozin for his patience and discussions, and to the peer reviewers for their valuable suggestions.

References

[1] T. R. Bader, A. M. Herneth, W. Blaicher, R. Steininger, F. Muhlbacher, G. Lechner, and F. Grabenwoger, "Hepatic perfusion after liver transplantation: Noninvasive measurement with dynamic single-section CT," *Radiology*, vol. 209, pp. 129–134, 1998.

[2] N. Sebastian and L. Gu, "A novel liver perfusion analysis method," in *Proc. 27th Annu. Conf. IEEE Eng. Med. Biol.*, 2005, pp. 3063–3066.

[3] G. Chen and L. Gu, "A novel liver perfusion analysis based on active contours and chamfer matching," in *Medical Imaging and Augmented Reality (Lecture Notes in Computer Science 4091)*. Berlin, Germany: Springer-Verlag, 2006, pp. 108–115.

[4] J. A. Sethian, "Level set methods and fast marching methods: Evolving interfaces in computational geometry, fluid mechanics," in *Computer Vision and Material Science*. Cambridge, U.K.: Cambridge Univ. Press, 1999.

[5] J. S. Suri, S. K. Setarehdan, and S. Singh, *Advanced Algorithmic Approaches to Medical Image Segmentation: State-ofthe- Art Applications in Cardiology, Neurology, Mammography and Pathology*. Berlin, Germany: Springer-Verlag, 2001.

[6] R. Malladi and J. A. Sethian, "Image processing via level set curvature flow," *Proc. Nat. Acad. Sci.*, vol. 92, no. 15, pp. 7046–7050, 1995.

[7] L. Hua, E. Abderrahim, F. Jaral, and R. Su, "An improved image segmentation approach based on level set and mathematical morphology," in *Proc. SPIE, 3rd Int. Symp. Multispectral Image Process. Pattern Recognit.*, Sep., 2003, vol. 5286, pp. 851–854.

[8] A. Evans, T. Lambrou, A. Linnery, and A. Todd-Pokroped, "Automatic segmentation of liver using a topology adaptive snake," in *Proc. Biomed. Eng.*, Innbruck Austria, 2004.

[9] F. Liu, B. Zhao, P. K. Kijewski, L. Wang, and L. H. Schwartz, "Liver segmentation for CT images using GVF snake," *Med. Phys.*, vol. 32, no. 12, pp. 3699–3706, 2005.

[10] C. Xu and J. L. Prince, "Gradient vector flow: A new external force for snakes," in *Proc. IEEE Proc. Conf. Comp. Vis. Pattern Recognit. (CVPR 1997)*, pp. 66–71.

[11] C. Xu and J. L. Prince, "Snakes, shapes, and gradient vector flow," *IEEE Trans. Image Process.*, vol. 7, pp. 359–369, Mar. 1998.

[12] M. Pham, R. Susomboon, T. Disney, D. Raicu, and J. Furst, "A comparison of texture models for automatic liver segmentation," presented at the SPIE Med. Imag. Conf., San Diego, CA, 2007.

[13] S. Geman and D. Geman, "Stochastic relaxation, gibbs distributions, and the bayesian restoration of images," *IEEE Trans. Pattern Anal. Mach. Intell.*, vol. 6, no. 6, pp. 721–741, Nov. 1998.

[14] S. J. Lim, Y. Y. Jeong, and Y. S. Ho, "Automatic liver segmentation for volume measurement in CT images," *JVCIR*, vol. 17, no. 4, pp. 860–875, 2006.

[15] F. Daisuke, S. Akinobu, and K. Hidefumi, "Automatic Liver Segmentation Method based on Maximum A Posterior Probability Estimation and Level Set Method," in *Proc. Med. Image Comput. Comput.-Assisted Intervention (MICCAI 2007) Workshop 3D Segmentation Clin.: Grand Challenge*, 2007, pp. 117–124.

[16] T. Okada, R. Shimada, Y. Sato, M. Hori, K. Yokota, M. Nakamoto, Y. Chen, H. Nakamura, and S. Tamura, "Automated segmentation of the liver from 3D CT images using probabilistic atlas and multi-level statistical shape model," in *Proc. Med. Image Comput. Comput.-Assisted Intervention (MICCAI 2007)*, pp. 86–93.

[17] T. Heimann, I. Wolf, and H. P. Meinzer, "Active shape models for a fully automated 3d segmentation of the liver—An evaluation on clinical data," in *Proc. Med. Image Comput. Comput.-Assisted Intervention (MICCAI 2006)*, pp. 41–48.

[18] M. Kass, A. Witkin, and D. Terzopolous, "Snake: Active contour models," in *Proc. 1st Int. Conf. Comput. Vis.*, 1987, pp. 259–268.

[19] T. Chan and L. Vese, "Active contours without edges," *IEEE Trans. Image Process.*, vol. 10, no. 2, pp. 266–277, Feb. 2001.

[20] H. G. Barrow, J. M. Tenenbaum, R. C. Bolles, and H. C. Wolf, "Parametric correspondence and chamfer matching: Two new techniques for image matching," in *Proc 5th Int. Joint Conf. Artif. Intell.*, 1997, pp. 659–663.

[21] G. Borgefors, "Hierarchical chamfer matching: A parametric edge matching algorithm," *IEEE Trans. Pattern Anal. Mach. Intell.*, vol. 10, no. 6, pp. 849–865, Nov. 1988.

[22] Y. Jin, A. F. Laine, and C. Imielinska, "An adaptive speed term based homogeneity for level set segmentation," in *Proc. Med. Imag. SPIE*, 2002, vol. 4684, no. 1, pp. 383–390.

[23] D. Adalsteinsson and J. Sethian, "A fast level set method for propagating interfaces," *J. Comput. Phys.*, vol. 118, pp. 269–277, 1995.

[24] M. H. Alsuwaiyel, *Algorithms Design Techniques and Analysis*. Singapore: World Scientific, 1998, pp. 471–474.

[25] J. O'Rourke, *Computational Geometry in C*. New York: Cambridge Univ. Press, 1994.

[26] K. H. Wong, J. W. VanMeter, S. T. Fricke, C. R. Maure, Jr., and K. Clearya, "MRI for modeling of liver and skin respiratory motion," in *Proc. CARS 2004*, pp. 747–752.
[27] T. Rohlfing, C. R. Maurer, Jr., W. G. O'Dell, and J. Zhong, "Modeling liver motion and deformation during the respiratory cycle using intensity-based free-from registration of gated MR images," in *Proc. SPIE*, 2001, vol. 4319, pp. 337–348.
[28] S. Osher and J. Sethian, "Fronts propagating with curvature-dependent speed: Algorithms based on hamilton-jacobi formulations," *J. Comput. Phys.*, vol. 79, pp. 12–49, 1998.
[29] R. Malladi and J. A. Sethian, "An O(N log N) algorithm for shape modeling," *Proc. Nat. Acad. Sci.*, vol. 93, pp. 9389–9392, 1996.
[30] R. Materne, B. E. Van Beers, A. M. Smith, I. Leconte, J. Jamart, J. P. Dehoux, A. Keyeux, and Y. Horsmans, "Non-invasive quantification of liver perfusion with dynamic computed tomography and a dual-input one-compartmental model," *Clin. Sci (London)*, vol. 99, pp. 517–525, 2000.
[31] V. Chalana and Y. Kim, "A methodology for evaluation of boundary detection algorithms on medical images," *IEEE Trans. Med. Imag.*, vol. 16, no. 5, pp. 642–652, Oct. 1997.
[32] C. E. Metz, "ROC methodology in radiologic imaging," *Investigative Radiol.*, vol. 21, pp. 720–733, 1986.
[33] F. Aaron and C. Bernard, "Evaluation of segmentation algorithms for medical imaging," in *Proc. 2005 IEEE Eng. Med. Biol. 27th Annu. Conf.*, Shanghai, China, Sep., pp. 7186–7189.

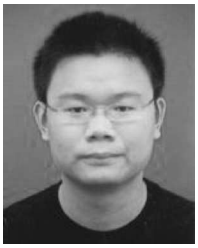

Gang Chen received the B.Sc. degree in computer science from Zhejiang University, Hangzhou, China, in 2005. He is currently working toward the M.Sc. degree in computer science at Shanghai Jiao Tong University, Shanghai, China.

His current research interests include medical image segmentation and validation.

Lixu Gu (M'00) received the Ph.D. degree in computer science from Toyohashi University of Technology, Toyohashi, Japan, in 1999.

He was a Research Associate at Robarts Research Institute for three years in image guided surgery and therapy, and was responsible for the development of the software for clinical applications. In 2003, he joined the Research Group in Computer Science, Shanghai Jiao Tong University, Shanghai, China, where he is currently a Professor of both computer science and Med-X Research Institute, directing the Image Guided Surgery and Therapy Laboratory. His current research interests include pattern recognition, computer vision, medical image processing, computer graphics, and image-guided surgery and therapy. He is the author or coauthor of more than 60 papers.

Prof. Gu is a Consultant Member of the Multimedia Branch of Shanghai Computer Association, a member of the Institute of Electrical and Electronics Engineers, and the Social Chair and a program committee (PC) member of the 27th IEEE Engineering in Medicine and Biology Society (EMBS) Conference, Shanghai. He was awarded the Best Poster in the 17th Congress of Computer Assisted Radiology and Surgery (CARS), London, U.K., in 2003. He is serving as an associate editor for both the IEEE Trans. on Information Technology for Biomedicine and the International Journal of Computer Assisted Radiology and Surgery. He is also a PC member of the CARS, the Medical Imaging and Augmented Reality (MIAR), and the Information Technology Applications in Biomedicine (ITAB) Conferences.

Lijun Qian received the M.D. degree from the Medical School, Shanghai Jiaotong University, Shanghai, China.

He is a Radiologist at Renji Hospital, Shanghai Jiao Tong University, Shanghai. His current research interests include hepatobiliary imaging, neuroradiology, and medical image processing.

Jianrong Xu received the M.D. degree from the Shanghai Medical University, Shanghai, China.

He is currently a Professor at Shanghai Jiao Tong University, Shanghai, where he is also the Chief of the Radiology Department, Renji Hospital, School of Medicine. Since 1983, he has been a Radiologist. His current research interests include skeletomuscular imaging, hepatobiliary imaging, neuroradiology, and imaging in rheumatic diseases and interventional procedures.